Integrated Metabolic Flux and Omics Analysis of *Leishmania major* metabolism

Sushil Shakyawar[1, 2], Isabel Rocha[1, 2], and Sonia Carneiro[1,*]

[1]SilicoLife Lda, Braga, Portugal
[2]University of Minho, Braga, Portugal
*Corresponding author: scarneiro@silicolife.com

Abstract

Leishmaniasis is a virulent parasitic infection that causes a significant threat to human health worldwide. The existing drugs are becoming less effective due to the ability of *Leishmania spp.* to alter its metabolism to adapt to harsh environments. Understanding how this parasite manipulates its metabolism inside the host (*e.g.* sandfly and human) might underpin new ways to prevent the disease and develop effective treatment strategies.
Despite significant advances in omics technologies, biochemistry of parasites still lacks the understanding of molecular components that determine the metabolic behavior under varying conditions. Metabolic network modeling might be of interest to identify physiologically relevant nodes in a metabolic network.

The present work proposes a metabolic model *i*SK570 (an extension of the *i*AC560 model) with additional reactions for the metabolism of lipids, long chain fatty acids and carbohydrates to study the metabolic behavior of this parasite. Gene Inactivity Moderated by Metabolism and Expression (GIMME) algorithm was used to verify the consistency between model flux predictions and gene expression data. Improved flux distributions were obtained, allowing a more accurate understanding of stage-specific metabolism in of promastigotes and amastigotes.

1. Introduction

Protozoan parasites from the genus *Leishmania* belong to the family Trypanosomatidae, and cause a spectrum of human diseases affecting around 12 million people worldwide (www.who.int). Existing treatment therapies involving drugs such as *e.g.* sodium stibogluconate and meglumine antimoniate, amphotericin B and miltefosine are limited by various features, including in some cases host toxicity and lack of efficacy [1,2]. Considering endemic severity of the disease, there is an urgent need for understanding *Leishmania* metabolism which can subsequently help in developing novel anti-leishmanial therapies.

Significant alterations have been observed in the metabolism exhibited by *Leishmania* at different stages of its life cycle, where it faces different nutritional environments [3]. For example, the promastigote form (inside sandfly) of *Leishmania* preferably uses glucose and L-proline via glycolysis pathways and TCA cycle; while amastigote uses glucosamine (GlcN) and its derivative N-acetylglucosamine (GlcNAc)along with some lipids and amino acids [4,5]. Availability of various sugars, such as hexoses (*e.g.* glucose, mannose, and galactose) and amino sugars (*e.g.* GlcN and GlcNAc) are determining factors for parasitic metabolic phenotype, especially for synthesizing essential glycans and glycoconjugates [6].

Unfortunately, no previous studies have explained the metabolic basis leading to the biosynthesis of glycans and glycoconjugates in the presence of different environments. In fact, it is still unknown if observed metabolic changes are resulting from, or arising out of the different parasitic stages. For example, under promastigote stage, only a few enzymes from the TCA cycle are active, while in amastigote stage, glycolytic enzymes are less functional.

Metabolic network modeling is an effective and sophisticated approach for systematically study the metabolic behaviour of an organism, as well as to understand the relationship between its genotype and phenotype. Previously, these methods have been used to understand the cellular metabolism as well as to identify essential genes in many medically important organisms, such as *Mycobacterium tuberculosis* [7], *Acinetobacter baumanii* [8], *Francisella tularensis* [9] including human parasites like *Leishmania major* [10] and *Plasmodium falciparum* [11]; though with the low prediction accuracy. One of the most probable and obvious reasons for the low prediction accuracy might be associated with the lack of use of experimental data (*e.g.* transcriptomics, proteomics, and metabolomics etc.) to constrain the model and unavailability of the suitable strategies to use omics data in the metabolic network analyses.

Integrating omics data with metabolic network analysis can improve our understanding on various aspects, such as metabolic alterations associated with the environmental conditions, essential genes and metabolic flux variability of the essential reactions [12]. The relevant data can be integrated into the metabolic model to provide an extra layer of metabolic flux constraints to improve its overall prediction efficiency. Various methods like GIMME [13], iMAT [14], MADE [15], E-Flux [15] and PROM [16] have been made available for the integration of transcriptomics and genomics, fluxomics [17], and metabolomics [18] data into metabolic models. Successful examples include the integration of RNAseq data into the *Leishmania infantum* model [19], proteomics data into a metabolic model of *Enterococcus faecalis* [20], and multi-omics data into metabolic models of *Escherichia coli* [21] to understand the metabolism and associated phenotypes. The strategy has also improved drug target predictions in many medically important organisms such as *Aspergillus fumigatus* [22], *Plasmodium falciparum* [23] and *L. major* [24].
In spite of the availability of abundant omics data and various methodologies, only a few studies have employed these strategies to understand the metabolism of *Leishmania* [10,19,25]. Here, we applied omics data with metabolic modeling approaches to understand the metabolic profile of *L.*

978-1-943436-11-8 / copyright ISCA, BICOB 2018
March 19-21, 2018, Las Vegas, Nevada, USA

major under different environmental conditions. The workflow mainly includes the integration of gene expression data from promastigote and amastigote stages into our metabolic model using Gene Inactivity Moderated by Metabolism and Expression (GIMME) method [13].

2. Methodology

2.1. Model extension and refinement

The existing metabolic model *i*AC560 [10] was extended to include sugar nucleotides biosynthetic pathways, which reactions and enzyme-coding genes were collected from databases like KEGG [26] and LeishCyc [27]. As some of the reaction steps were not associated with a specific gene, homology search tools like BLAST [1], were applied to find the highest scoring gene sequences (% identity ≥ 40%, alignment length ≥ 70% and E-value $1.0e^{-30}$), as described in [19] and associate those to the corresponding reactions. Additionally, based on experimental evidence, several metabolic reactions were altered in terms of reversibility and/or compartments, while new transport reactions for sugar nucleotides, lipids, and fatty acids were also included. Refer to **Supplementary material S1** for added, deleted or altered reactions.

2.2. Biomass composition

The macromolecular composition of *L. major* cells was also corrected. Protein, DNA and RNA contents were estimated from *L. donovani* studies [19], while carbohydrates, lipids, and polyamine contents were calculated using experimental data from protozoan *Tetrahymena* [28,29] and *L. mexicana* [30]. Individual carbohydrates, such as mannan, lipophosphoglycan (LPG), glycoinositol phospholipid (GIPL), and N-glycans, were estimated as follows: mannan contents were assumed to represent 80% and 90 % of all carbohydrates in promastigote and amastigote stage, respectively [30], while LPG, GIPL, and N-glycans would represent 20% and 10% in total, respectively. The relative mass fractions (w/w) of LPG, GIPL, and N-glycans were estimated based on previous studies [31–34]. Further details on biomass calculations can be found in **Supplementary material S2.**

2.3. In-silico media formulation

2.3.1. Modified Media for Promastigote (MMP)

MMP was formulated for *L. major* growth under promastigote stage, which includes 16 nutrient sources: L-arginine, L-cysteine, L-histidine, L-isoleucine, L-leucine, L-lysine, L-methionine, L-phenylalanine, L-threonine, L-tyrosine, L-valine, hypoxanthine, phosphate, oxygen, proline, and glucose. The nutrients, in particular, glucose and proline were considered based on the previous studies [35,36], explaining that both the compounds are major carbon source for *Leishmania* promastigote, while remaining ones were included considering the experimental studies [37,38] and computational predictions in [10], which concluded that *Leishmania* can grow in these nutrients.

2.3.2. Modified Media for Amastigote (MMA)

MMA includes all 16 nutrients from MMP with additional amino sugars, amino acids, lipids and fatty acids, making a total of 21 nutrients. GlcN and GlcNAc sugars were added considering findings from Naderer et al. (2010) studies [4] that showed the degradation of glycosaminoglycans inside macrophages to provide GlcN and GlcNAc as carbon sources during the amastigote stage. Fatty acids like stearyl acid and lipids, *e.g.* phosphatidylethanolamine were also considered, based on different studies that show that *Leishmania* utilizes lipids from host cells and transports them into the cytosol [39,40]. The consumption of the lipids and fatty acids during amastigote stages were also supported by other experimental studies discussing the possibility of growth of *Leishmania* axenic amastigote in lipid and fatty acid-rich medium [41–43]. The amino acids aspartate and alanine were also added to MMA, based on higher consumption measurements of these amino acids as carbon sources by amastigotes [44].

2.4. Reaction flux constraints in FBA-based simulations

Model simulations under amastigote and promastigote stages were estimated using different reaction constraints. For example, the uptake flux for proline was reduced by 90% in amastigote compared to promastigote simulations, based on the previous study showing a decrease in the consumption of this particular amino acid in *L. mexicana* amastigotes [35]. Also, glucose uptake flux was constrained to 90% less than that in the promastigote stage, considering previous findings [45,46], which concluded that parasitophorous vacuole is a compartment poor in glucose. Furthermore, the oxygen uptake in amastigote stage was significantly reduced as compared to that in the promastigote stage, considering the fact that *Leishmania*-infected macrophage is an oxygen-deficient entity [47,48]. The upper and lower limits for uptake fluxes for all other nutrients were set unconstrained (See **Supplementary material S2**).

2.5. Metabolic network analysis

The gene expression data (FPKM[1] values) of 10275 genes from *Leishmania* spp. [49] was integrated with the extended metabolic model (termed as *i*SK570) by applying GIMME approach. OptFlux modules [50] were used to run GIMME algorithm and to perform FBA-based analyses under different environmental conditions.

Briefly, GIMME implementation considers genes (and associated reactions) with an expression level below the threshold as inactive, and thus removes those from the simulation. The algorithm may reconsider few of these

[1] FPKM (Fragments Per Kilobase Million) is method for estimating relative abundance of transcripts in terms of fragments observed in RNA-Seq experiment.

inactive reactions, especially the essential ones and so-called metabolically important reactions (MIRs), back in the simulation to achieve an optimal solution. The remaining reactions are blocked and termed as metabolically unwanted reactions (MURs) in that particular metabolic state. Inconsistencies between the metabolic model and gene expression data are estimated based on MIRs that are re-inserted in the model; however, GIMME solves a linear programming (LP) on reconsidered reactions to minimize this inconsistency. As such, inconsistency scores (IS) are calculated and associated with each metabolic reaction. Accordingly, metabolic reactions can be categorized as follow:

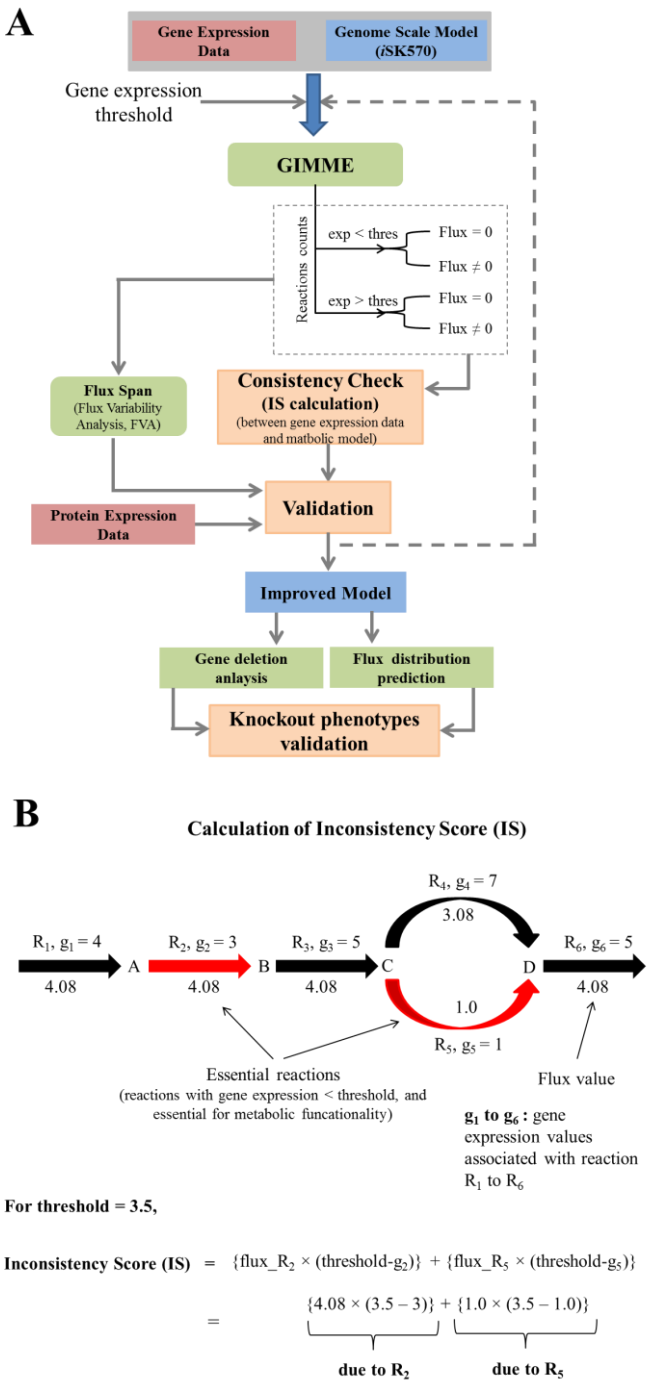

Figure 1: A) Workflow for integrating gene expression data into the metabolic. **B)** An exemplifying scheme for calculating inconsistency score (IS) using gene expression and flux values.

(1) inactive (expression levels below the threshold and metabolic flux[2] equal to zero);
(2) potentially inactive (expression levels below the threshold and metabolic flux[2] is non-zero);
(3) potentially active (expression levels above the threshold and metabolic flux[2] equal to zero);
(4) active (expression levels above the threshold and metabolic flux[2] is non-zero).

Different threshold values were tested, and inconsistency scores (IS) were recalculated as described in [13] (**Figure 1**). Furthermore, flux spans[3] based on Flux Variability Analysis (FVA) and PFBA flux distributions were compared. The predicted changes in metabolic operability of reactions after GIMME implementation were also compared with proteomic data from Pawar et al. (2014) [51].

3. Results and Discussion

3.1. Consistency between metabolic model *i*SK570 and gene expression data in promastigote conditions

Based on different tests, where the gene expression threshold values were changed, it was observed that IS values increase with the threshold values (**Figure 2A**), particularly above threshold values of 11 (**Figure 2B**). Below this threshold, IS values are close to zero, indicating that there are only a few inconsistencies between predicted fluxes and gene expression levels associated to the corresponding reactions. As such, while increasing the threshold value more reactions with predicted fluxes different from zero, but with low expression levels, i.e. reactions that should be active, are included, which increases the level of inconsistency between expression data and flux predictions. Although the number of potentially inactive reactions, i.e. reactions with expression levels below the threshold and predicted zero flux, increases with the threshold value, agreeing with metabolic predictions; the fact is that increasing the threshold value tends to exclude reactions that should be active as predicted by FBA-based simulations.

[2] Metabolic flux was calculated by performing GIMME which uses Parsimonious Flux Balance Analysis (PFBA) to run simulations.
[3] Flux span refers to the difference between maximum and minimum flux values that a reaction can carry according to FVA analysis.

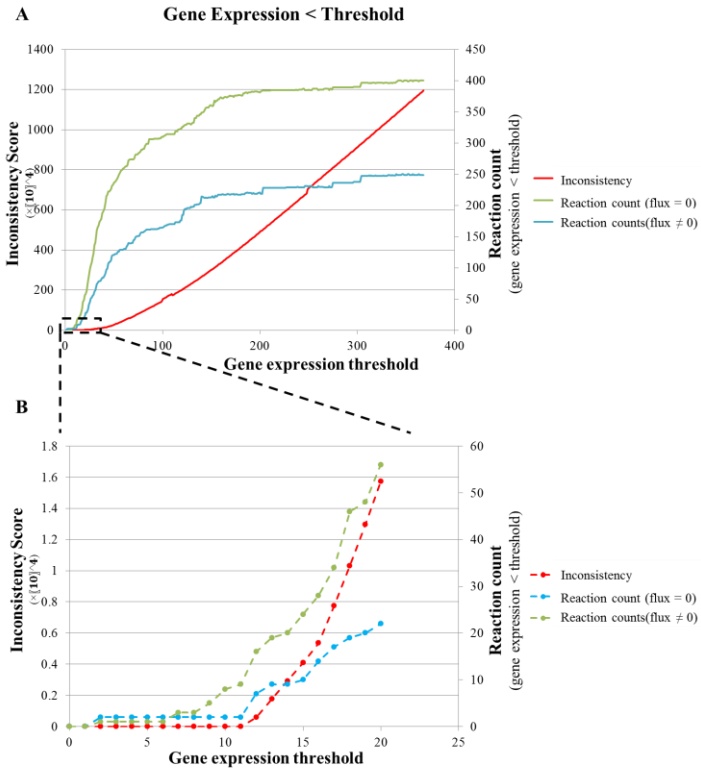

Figure 2: Evaluating inconsistencies between *i*SK570 model predictions and gene expression data from *L. major* promastigote cells. **A)** Inconsistency scores (IS) were calculated for different expression threshold values, while estimating the number of reactions with gene expression levels below a threshold value and predicted flux values equal and different from zero. **B)** Zoom in of plot A for lower threshold values, showing the variation in the inconsistency score and the number of reactions with gene expression below threshold flux values different and equal to zero.

As shown in **Figure 2A,** the number of potentially inactive reactions (i.e. with gene expression less than the threshold and predicted flux equal to zero) increases to a maximum of 400 at the highest expression threshold value (368). In general, GIMME considers these reactions as MURs (or metabolically unwanted reactions) and, ultimately they do not have an impact on the flux distribution. Similarly, potentially active reactions (i.e. with gene expression less than threshold and flux equal to zero) can be associated with MIRs and GIMME might need to reconsider some of these reactions during the simulation process. These are almost 250 at a maximum threshold value of 368. Although the number of MIRs are lower than the number of MURs at a particular threshold value, these contribute far more to increase IS values. Therefore a threshold value should be carefully selected. In the following analysis, a threshold value of 12 (equivalent IS = 5.9×10^{2}) was chosen to perform GIMME simulations, which predicted 30 genes (out of 570) with expression levels below the threshold value, corresponding to 23 reactions from which 16 were considered MURs and 7 MIRs.

3.2. FVA and PFBA analyses

FVA analyses were performed based on GIMME results using a threshold value of 12. Briefly, the idea was to evaluate changes in metabolic predictions imposed by GIMME constraints (especially blocked reactions or MURs) and estimate the impact in the predicted metabolic flexibility under the defined conditions. Therefore, FVA analyses with and without GIMME constraints were compared. Reactions were categorized as such: type1, minimum and maximum FVA fluxes equal to zero; type2, minimum and maximum FVA fluxes different from zero (either positive or negative); and type3, minimum and maximum FVA fluxes equal to upper and lower bounds of reactions (**Table 1**).
Results show that the number of reactions type3 decreased, while reactions type1 and type2 increased, which suggests that GIMME-based constraints reduced metabolic flexibility associated with large FVA spans as defined by FVA fluxes of type 3 reactions. Also, reactions type 1 with FVA spans of zero (i.e. blocked reactions) contribute to decrease this metabolic flexibility, as the number of possible alternatives for carbon distribution within the network also decreases. Minimum and maximum flux values from FVA analyses with and without GIMME constraints for each reaction are presented in **Supplementary material S1.**

Table 1: Number of reactions classified as type1, type2 and type3 from FVA results considering simulations with and without GIMME-based constraints (i.e. deleting MURs).

Reaction Category	Minimum (min) and maximum (max) FVA values	Number of reactions	
		Without GIMME-based constraints	With GIMME-based constraints
type1	min = 0 and max = 0	472	493
type2	min/max< 0 or min/max > 0	239	256
type3	min =lower bound and max=upper bound	466	428

Additionally, PFBA and GIMME flux distributions were compared. In general, flux distributions did not change significantly, most likely because of small differences in the number of active and non-active reactions (**Figure 3A**); however, few reactions changed their flux values from zero to non-zero and vice-versa. The reactions with these binary changes are mostly transport reactions, but reactions associated with metabolic pathways like "Glycerolipid metabolism" (30.3 %) and "Pyrimidine metabolism" (9.09%) (**Figure 3B**) were also found. Changes in flux operability of these reactions can be supported by proteomic data for *L. major* from Pawar et al., 2014 [51], which showed that genes associated with eight reactions (out of ten) that changed their fluxes from zero to non-zero, are expressed at the protein level (**Table 2**). This indicates that GIMME-based flux analyses improve model predictions.

Table 2: List of reactions which showed binary changes (zero to non-zero) in their fluxes after GIMME implementation (threshold value of 12), and which associated enzymes have positive expression at protein level.

Reaction ID	PFBA flux value		Associated genes	Protein expression [51]
	Without GIMME	With GIMME		
R_AGPATi_LM	0	4.80	LmjF32.1960	yes
R_CDPDSPm_LM	0	3.26	LmjF14.1200	yes
R_GPAM_LM	0	4.80	LmjF34.1090	yes
R_HEXg	0	99.30	(LmjF21.0250 or LmjF36.2320) or LmjF21.0240)	yes
R_ME1x	0	162.49	LmjF24.0770	yes
R_PAPAm_LM	0	1.04	(LmjF18.0440 or LmjF19.1350)	yes
R_PNS1	0	10000	LmjF29.2800	yes
R_UPPRTr	0	-10000	LmjF34.1040	yes

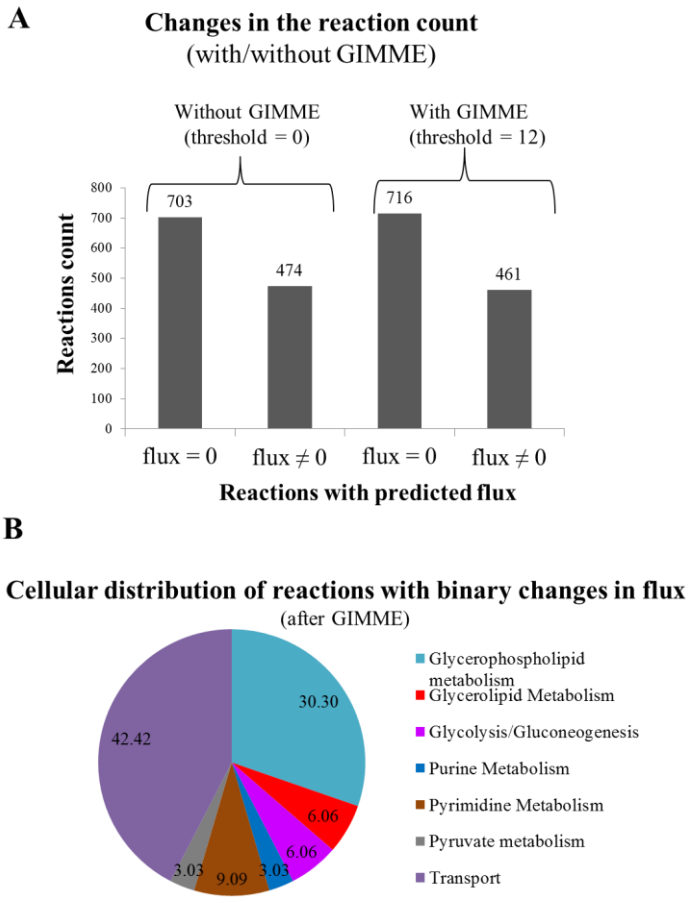

Figure 3: A) Changes in the number of reactions with predicted flux = 0 or ≠ 0 after GIMME implementation. **B)** Percentage cellular distribution of the reactions which showed binary changes in their fluxes after GIMME.

4. Conclusion

The work described the application of GIMME algorithm in combination with flux-based analysis to integrate gene expression data into genome-scale models to determine consistency between data and metabolic model *i*SK570. The strategy has been used to put an extra layer of stoichiometric constraints on reactions to predict more accurate fluxes across various pathways of *L. major*. The predicted activation/inactivation of the metabolic reactions in a particular environment was supported by expression of the associated enzymes at the protein level. Improved flux distribution further used to describe stage-specific metabolism and drug target predictions in *Leishmania* (not described here due to page limitations). All supplementary data mentioned in this manuscript can be provided on demand.

5. Funding and Acknowledgement

This work was supported by the Initial Training Network, GlycoPar, funded by the FP7 Marie Curie Actions of the European Commission (FP7-PEOPLE-2013-ITN-608295). The authors gratefully express appreciation to SilicoLife Lda for providing required infrastructural facilities related to this work. We also thank Bruno Pereira (systems biologist at SilicoLife) and Hugo Giesteira (programmer at SilicoLife) for scientific and technical assistance during various phases of the project.

6. References

1. Philippe J. Guerin, Piero Olliaro, Shyam Sundar, Marleen Boelaert, Simon L. Croft, Philippe Desjeux, Monique K. Wasunna, and Anthony D.M. Bryceson. Visceral leishmaniasis: current status of control, diagnosis, and treatment, and a proposed research and development agenda. *Lancet Infect. Dis*, 2:494–501, 2002.
2. Goto H, Lindoso JA. Current diagnosis and treatment of cutaneous and mucocutaneous leishmaniasis. Expert Rev Anti Infect Ther, 8:419–433, 2010.
3. Fred R. Opperdoes and Graham H. Coombs. Metabolism of Leishmania: proven and predicted. Trends Parasitol, 23:149–158, 2007.
4. Thomas Naderer, Joanne Heng, and Malcolm J. McConville. Evidence that intracellular stages of Leishmania major utilize amino sugars as a major carbon source. PLoS Pathog, 6, 2010.
5. Thomas Naderer, Miriam Ellis, M Fleur Sernee, David P. De Souza, Joan Curtis, Emanuela Handman, and Malcolm J. McConville. Virulence of Leishmania major in macrophages and mice requires the gluconeogenic enzyme fructose-1,6-bisphosphatase. Proc. Natl. Acad. Sci. U. S. A., 103:5502–5507, 2006.
6. Daniel C. Turnock and Michael A. J. Ferguson. Sugar nucleotide pools of Trypanosoma brucei, Trypanosoma cruzi, and Leishmania major. Eukaryot. Cell, 6:1450–1463, 2007.
7. Dany J. V. Beste, Tracy Hooper, Graham Stewart, Bhushan Bonde, Claudio Avignone-Rossa, Michael E. Bushell, Paul Wheeler, Steffen Klamt, Andrzej M. Kierzek, and Johnjoe McFadden. GSMN-TB: a web-based genome-scale network model of Mycobacterium tuberculosis metabolism. Genome Biol., 8:R89, 2007.
8. Hyun U. Kim, Tae Y. Kim, and Sang Y. Lee. Genome-scale metabolic network analysis and drug targeting of multi-drug resistant pathogen Acinetobacter baumannii AYE. Mol. Biosyst., 6:339–48, 2010.
9. Anu Raghunathan, Sookil Shin, and Simon Daefler. Systems approach to investigating host-pathogen interactions in infections with the biothreat agent Francisella. Constraints-based model of Francisella tularensis. BMC Syst. Biol., 4:118, 2010.
10. Arvind K. Chavali, Jeffrey D. Whittemore, James A. Eddy, Kyle T.

Williams, and Jason A. Papin. Systems analysis of metabolism in the pathogenic trypanosomatid Leishmania major. Mol. Syst. Biol., 4:177, 2008.
11. Germán Plata, Tzu Lin Hsiao, Kellen L. Olszewski, Manuel Llinás, and Dennis Vitkup. Reconstruction and flux-balance analysis of the Plasmodium falciparum metabolic network. Mol. Syst. Biol., 6:408, 2010.
12. Rajib Saha, Anupam Chowdhury, and Costas D. Maranas. Recent advances in the reconstruction of metabolic models and integration of omics data. Curr. Opin. Biotechnol., 29:39–45, 2004.
13. Scott A. Becker and Bernhard O. Palsson. Context-specific metabolic networks are consistent with experiments. PLoS Comput. Biol., 4, 2008.
14. Tomer Shlomi, Moran N. Cabili, Markus J. Herrgård, Bernhard Palsson, and Eytan Ruppin. Network-based prediction of human tissue-specific metabolism. Nat. Biotechnol., 26:1003–1010, 2008.
15. Paul A. Jensen and Jason A. Papin. Functional integration of a metabolic network model and expression data without arbitrary thresholding. Bioinformatics, 27:541–547, 2011.
16. Sriram Chandrasekaran and Nathan D. Price. Probabilistic integrative modeling of genome-scale metabolic and regulatory networks in Escherichia coli and Mycobacterium tuberculosis. Proc. Natl. Acad. Sci. U. S. A., 107:17845–50, 2010.
17. Sharon J. Wiback, Radhakrishnan Mahadevan, and Bernhard Palsson. Using Metabolic Flux Data to Further Constrain the Metabolic Solution Space and Predict Internal Flux Patterns: The Escherichia coli Spectrum. Biotechnol. Bioeng., 86:317–331, 2004.
18. Tunahan Cakir, Kiran R. Patil, Zeynep I. Onsan, Kutlu O. Ulgen, Betul Kirdar, and Jens Nielsen. Integration of metabolome data with metabolic networks reveals reporter reactions. Mol. Syst. Biol., 2:50, 2006.
19. Mahesh Sharma, Naeem Shaikh, Shailendra Yadav, Sushma Singh, and Prabha Garg. A systematic reconstruction and constraint-based analysis of Leishmania donovani metabolic network: identification of potential antileishmanial drug targets. Mol. BioSyst., 277:38245–38253, 2017.
20. Ruth Großeholz, Ching-Chiek Koh, Nadine Veith, Tomas Fiedler, Madlen Strauss, Brett Olivier, Ben C. Collins, Olga T. Schubert, Frank Bergmann, Bernd Kreikemeyer, Ruedi Aebersold, and Ursula Kummer. Integrating highly quantitative proteomics and genome-scale metabolic modeling to study pH adaptation in the human pathogen Enterococcus faecalis. npj Syst. Biol. Appl., 2:16017, 2016.
21. Andrew R. Joyce and Bernhard O. Palsson. The model organism as a system: integrating 'omics' data sets. Nat. Rev. Mol. Cell Biol., 7:198–210, 2006.
22. Martin Kaltdorf, Mugdha Srivastava, Shishir K. Gupta, Chunguang Liang, Jasmin Binder, Anna-Maria Dietl, Zohar Meir, Hubertus Haas, Nir Osherov, Sven Krappmann, and Thomas Dandekar. Systematic identification of anti-fungal drug targets by a metabolic network approach. Front. Mol. Biosci., 3:1–19, 2016.
23. Philipp Ludin, Ben Woodcroft, Stuart A. Ralph, and Pascal Mäser. In silico prediction of antimalarial drug target candidates. Int J Parasitol Drugs Drug Resist, 2:191–199, 2012.
24. Arvind K. Chavali, Anna S. Blazier, Jose L. Tlaxca, Paul A. Jensen, Richard D. Pearson, and Jason A. Papin. Metabolic network analysis predicts efficacy of FDA-approved drugs targeting the causative agent of a neglected tropical disease. BMC Syst. Biol., 6:27, 2012.
25. Abhishek Subramanian and Ram R. Sarkar. Revealing the mystery of metabolic adaptations using a genome scale model of Leishmania infantum. Sci. Rep., 7:10262, 2017.
26. Kanehisa M, Goto S. Kyoto Encyclopedia of Genes and Genomes. Nucleic Acids Res., 28:27–30, 2000.
27. Maria A. Doyle, James I. MacRae, David P. De Souza, Eleanor C. Saunders, Malcolm J. McConville, and Vladimir A. Likic. LeishCyc: a biochemical pathways database for Leishmania major. BMC Syst. Biol., 3:57, 2009.
28. Michael A. Gates, Andrew Rogerson, and Jacques Berger. Dry to wet weight biomass conversion constant for Tetrahymena elliotti (Ciliophora, Protozoa). Oecologia, 55:145–148, 1982.
29. P Hellung-Larsen and a P Andersen. Cell volume and dry weight of cultured Tetrahymena. J. Cell Sci., ; 92 (Pt 2):319–24, 1989.
30. Julie E. Ralton, Thomas Naderer, Helena L. Piraino, Tanya A. Bashtannyk, Judy M. Callaghan, and Malcolm J. McConville. Evidence that Intracellular???1-2 Mannan Is a Virulence Factor in Leishmania Parasites. J. Biol. Chem., 278:40757–40763, 2003.
31. Salvatore J. Turco and David L. Sacks. Expression of a stage-specific lipophosphoglycan in Leishmania major amastigotes. Mol. Biochem. Parasitol., 45:91–99, 1991.
32. Malcolm J. McConville and Mike Ferguson. The structure, biosynthesis and function of glycosylated phosphatidylinositols in the parasitic protozoa and higher eukaryotes. Biochem. J., 294:305–324, 1993.
33. Albert Descoteaux and Salvatore J. Turco. The lipophosphoglycan of Leishmania and macrophage protein kinase C. Parasitol. Today, 9:468–471, 1993.
34. John A. Kink and Kwang P. Chang. N-Glycosylation as a biochemical basis for virulence in Leishmania mexicana amazonensis. Mol. Biochem. Parasitol., 27:181–190, 1988.
35. Hart DT, Graham H. Coombs. Leishmania mexicana: Energy metabolism of amastigotes and promastigotes. Exp. Parasitol., 54:397–409, 1982.
36. Petrie M. Rainey and Nicholle Mackenzie. A carbon-13 nuclear magnetic resonance analysis of the products of glucose metabolism in Leishmania pifanoi amastigotes and promastigotes. Mol. Biochem. Parasitol., 45:307–315, 1991.
37. Timothee Merlen, Denis Sereno, Nathalie Brajon, Florence Rostand, and Jean Loup Lemesre. Leishmania spp.: Completely defined medium without serum and macromolecules (CDM/LP) for the continuous in vitro cultivation of infective promastigote forms. Am. J. Trop. Med. Hyg, 60:41–50, 1999.
38. Frederick L. Schuster and James J. Sullivan. Cultivation of clinically significant hemoflagellates. Clin. Microbiol. Rev., 15:374–389, 2002.
39. Thomas Naderer and Malcolm J. McConville. The Leishmania-macrophage interaction: A metabolic perspective. Cell. Microbiol., 10:301–308, 2008.
40. Kai Zhang, Justine M. Pompey, Fong F. Hsu, Phillip Key, Padmavathi Bandhuvula, Julie D. Saba, John Turk, and Stephen M. Beverley. Redirection of sphingolipid metabolism toward de novo synthesis of ethanolamine in Leishmania. EMBO J., 26:1094–104, 2007.
41. Malcolm J. McConville and Blackwell JM. Developmental changes in the glycosylated phosphatidylinositols of Leishmania donovani. Characterization of the promastigote and amastigote glycolipids. J. Biol. Chem., 266:15170–15179, 1991.
42. Winter G, Fuchs M, McConville MJ, et al. Surface antigens of Leishmania mexicana amastigotes: characterization of glycoinositol phospholipids and a macrophage-derived glycosphingolipid. J. Cell Sci., 107:2471–82, 1994.
43. Kai Zhang, Fong F. Hsu, David A. Scott, Roberto Docampo, John Turk, and Stephen M. Beverley. Leishmania salvage and remodelling of host sphingolipids in amastigote survival and acidocalcisome biogenesis. Mol. Microbiol., 55:1566–1578, 2005.
44. Eleanor C. Saunders, William W. Ng, Jennifer M. Chambers, Milica Ng, Thomas Naderer, Jens O. Krömer, Vladimir A. Likic, and Malcolm J. McConville. Isotopomer profiling of Leishmania mexicana promastigotes reveals important roles for succinate fermentation and aspartate uptake in Tricarboxylic Acid Cycle (TCA) anaplerosis,,glutamate synthesis, and growth. J. Biol. Chem., 286:27706–27717, 2011.
45. Henry W. Murray, Jonathan D. Berman, Clive R. Davies, and Nancy G. Saravia. Advances in leishmaniasis. Lancet, 366:1561–1577, 2005.
46. A Garami and T Ilg. The Role of Phosphomannose Isomerase in Leishmania mexicana Glycoconjugate Synthesis and Virulence. J. Biol. Chem., 276:6566–6575, 2001.
47. Alexander Mahnke, Robert J. Meier, Valentin Schatz, Julian Hofmann, Kirstin Castiglione, Ulrike Schleicher, Otto S. Wolfbeis, Christian Bogdan, and Jonathan Jantsch. Hypoxia in Leishmania major skin lesions impairs the NO-dependent leishmanicidal activity of macrophages. J. Invest. Dermatol., 134:2339–2346, 2014.
48. A. Degrossoli, Wagner W. Arrais-Silva, M. C. Colhone, F. R. Gadelha, P. P. Joazeiro and S. Giorgio. The Influence of Low Oxygen on Macrophage Response to Leishmania Infection. Scand. J. Immunol., 74:165–175, 2011.
49. Alberto Rastrojo, Fernando Carrasco-Ramiro, Diana Martín, Antonio Crespillo, Rosa M. Reguera, Begoña Aguado, and Jose M. Requena. The transcriptome of Leishmania major in the axenic promastigote stage: transcript annotation and relative expression levels by RNA-seq. BMC Genomics, 14:223, 2013.
50. Isabel Rocha, Paulo Maia, Pedro Evangelista, Paulo Vilaça, Simão Soares, José P. Pinto, Jens Nielsen, Kiran R. Patil, Eugénio C. Ferreira, and Miguel Rocha. OptFlux: an open-source software platform for in silico metabolic engineering. BMC Syst. Biol., 4:45, 2010.
51. Harsh Pawar, Santosh Renuse, Sweta N. Khobragade, Sandip Chavan, Gajanan Sathe, Praveen Kumar, Kiran N. Mahale, Kalpita Gore, Aditi Kulkarni, Tanwi Dixit, Rajesh Raju, T. S. Keshava Prasad, H. C. Harsha, Milind S. Patole, and Akhilesh Pandey. Neglected Tropical Diseases and Omics Science: Proteogenomics Analysis of the Promastigote Stage of Leishmania major Parasite. OMICS, 18:1–14, 2014.